The Solid-State Electrochemistry of Metal Octacyanomolybdates, Octacyanotungstates, and Hexacyanoferrates Explained on the Basis of Dissolution and Reprecipitation Reactions, Lattice Structures, and Crystallinities

Uwe Schröder[†] and Fritz Scholz*

Institut für Chemie und Biochemie, Ernst-Moritz-Arndt-Universität, Soldmannstrasse 23, 17489 Greifswald, Germany

Received August 4, 1999

The electrochemical behavior of solid microparticles of metal (Ag^+, Cd^{2+}, Co^{2+}, Cr^{2+}, Cu^{2+}, Fe^{2+}, Mn^{2+}, Ni^{2+}, Pb^{2+}, and Zn^{2+}) octacyanomolybdates, octacyanotungstates, and hexacyanoferrates has been studied by voltammetry, electrochemical quartz crystal microbalance, and microscopic diffuse reflectance spectroelectrochemical measurements. The solid microparticles have been immobilized on the surface of graphite electrodes prior to the electrochemical measurements. A comparative study of the cyclic oxidation and reduction of these compounds in the presence of potassium ions revealed that any interpretation of the electrochemistry requires the solubility equilibria of the reduced compounds to be taken into account , such as in the case of the silver salts $\{Ag_3K[X]\}$ and $\{Ag_4[X]\}$ (with $X = Fe^{II}(CN)_6^{4-}$, $M^{IV}(CN)_8^{4-}$ (M = Mo, W)). Because $\{Ag_4[X]\}$ has a lower solubility than $\{Ag_3K[X]\}$, the electrochemistry is accompanied by a conversion of solid $\{Ag_3K[X]\}$ into solid $\{Ag_4[X]\}$. Two distinct voltammetric signal systems are generated by these two compounds according to $\{Ag_3K[X]\} \rightleftarrows \{Ag_3[X]\} + K^+ + e^-$ and $\{Ag_4[X]\} \rightleftarrows \{Ag_3[X]\} + Ag^+ + e^-$. When silver ions are present in the solution adjacent to the microparticles, the silver octacyanometalates and silver hexacyanoferrate show a chemically reversible and very stable voltammetric behavior. Despite the fact that the electrochemistry is based upon a single-electron/single-ion transfer reaction ($\{Ag_4[X]\} \rightleftarrows \{Ag_3[X]\} + Ag^+ + e^-$), more than one electrochemical signal is observed because of the simultaneous presence of amorphous and crystalline particles. This study shows that the interplay of solubility equilibria and electrochemical equilibria is generally observed for the other metal octacyanomolybdates, octacyanotungstates, and hexacyanoferrates as well.

Introduction

Solid-state electrochemical reactions, which are not confined to only the surface, are accompanied by ion-transfer processes between the redox-active solid phase and the adjacent electrolyte solution.[1,2] The reason for this ion transfer is to maintain the electroneutrality found inside the solid phase. Such ion insertion/expulsion processes require a scaffold, which forms a tunnel or layer structure to enable the ion transport inside the solid phase. All very sparingly soluble metal octacyanomolybdates, octacyanotungstates, and hexacyanoferrates, considered in this work, possess a so-called zeolitic structure with channels and accessible cavities for ion transport and housing. This is a prerequisite for their insertion electrochemistry with a coupled electron and ion transfer.

Although the electrochemistry of metal hexacyanoferrates has been extensively studied,[3−9,15,30] several experimental results could not be explained thus far, such as, for example, the origin of some voltammteric signals, their shape and stability. However, a clear understanding of all electrochemical reactions is necessary as several metal cyanometalates find applications in sensors, electrochromic displays, electrocatalysis, and so forth. It is very interesting to compare the electrochemistry of solid metal octacyanomolybdates (*ocm*), octacyanotungstates (*oct*), and hexacyanoferrates *(hcf)*, as such study reveals common features that have yet to be described. The electrochemistry of the *dissolved* anions comprises a single electron-transfer step: $[Fe^{II}(CN)_6]^{4-} \rightleftarrows [Fe^{III}(CN)_6]^{3-} + e^-$ and $[M^{IV}(CN)_8]^{4-} \rightleftarrows [M^{V}(CN)_8]^{3-} + e^-$. Although the solution chemistry and electrochemistry of the hexacyanoferrates and octacyanometalates have been the subjects of thorough investigations,[10,11] little is known about the physical, chemical, and electrochemical properties of solid octacyanometalates. Cox et al. described a chemical irreversibility of the cyclic oxidation and reduction

* To whom correspondence should be addressed. Tel: +49(03834)-864450. Fax: +49(03834)864451. E-mail: fscholz@mail.uni-greifswald.de.
[†] Current address: Theoretical and Physical Chemistry Department, Oxford University, South Parks Road, OX1 3QZ, UK.

(1) Schöllhorn, R. *Angew. Chem.* **1980**, *92*, 1015; Schöllhorn, R. *Angew. Chem., Int. Ed. Engl.* **1980**, *19*, 983.
(2) Bruce, P. G., Ed. *Solid State Electrochemistry*; Cambridge University Press: Cambridge, England, 1995.
(3) Dostal, A.; Meyer, B.; Scholz, F.; Schröder, U.; Bond, A. M.; Marken, F.; Shaw, Sh. J. *J. Phys. Chem.* **1995**, *99*, 9, 2096−2103.
(4) Kahlert, H.; Retter, U.; Lohse, H.; Siegler, K.; Scholz, F. *J. Phys. Chem. B* **1998**, *44*, 8757−8765.
(5) Dostal, A.; Schröder, U.; Scholz, F. *Inorg. Chem.* **1995**, *34*, 1711−1717.
(6) Xidis, A.; Neff, V. D. *J. Electrochem. Soc.* **1991**, *138*, 3637.
(7) Feldmann, B. J.; Murray, R. W. *Inorg. Chem.* **1987**, *26*, 1702.
(8) Kulesza, P. J.; Malik, M. A.; Berrettoni, M.; Giorgetti, M.; Zamponi, S.; Schmidt, R.; Marassi, R. *J. Phys. Chem. B* **1998**, *102*, 1870−1876.
(9) Kulesza, P. J.; Faszynska, M. *J. Electroanal. Chem.* **1988**, *252*, 461−466.
(10) Samotus, A.; Szklarzewicz, J. *Coord. Chem. Rev.* **1993**, *125*, 63−74.
(11) Oyama, N.; Ohsaka, T.; Yamamoto, N.; Matsui, J.; Hatozaki O. *J. Electroanal. Chem.* **1989**, *265*, 297−304.
(12) Cox, J. *Anal. Chem.* **1985**, *57*, 2739−2740.
(13) (a) Scholz, F.; Meyer, B. Voltammetry of Solid Microparticles Immobilized on Electrode Surfaces. In *Electroanalytical Chemistry*; Bard, A., Rubinstein, I., Eds.; Marcel Dekker: New York, 1998; Vol. 20. (b) Voltammetry of Microparticles. www.iic.cas.cz/~grygar/AbrSV.html.

10.1021/ic9909330 CCC: $19.00
Published on Web 02/18/2000

of films of silver octacyanomolybdate, which appeared to be a peculiarity of silver octacyanomolybdate and tungstate.[12]

Here, it will be shown that the electrochemistry of these complex cyanides is strongly affected by the solubility equilibria of the involved compounds. It will be demonstrated that the complex and chemically irreversible electrochemistry of silver octacyanomolybdate in the presence of potassium ions, as observed by Cox et al.,[12] is caused by the competition of the solubility equilibria of $Ag_4[Mo^{IV}(CN)_8]$ and $Ag_3K[Mo^{IV}(CN)_8]$. This gives rise to an internal reprecipitation process accompanied by a partial dissolution. Under certain conditions, analogous reactions can also be observed in case of silver hexacyanoferrate and several other solid-metal hexacyanoferrates and octacyanometalates. However, these reactions differ to some extent because of the different structures of the solid compounds.

For this study, the *voltammetry of microcrystals* proved to be the most useful electroanalytical technique because it enabled us to investigate a wide number of synthesized compounds that could easily be characterized using the necessary analytical methods.[13] This is a great advantage over electrodes, on the surface of which films of compounds have been deposited by chemical or electrochemical methods.

Experimental Section

Electrochemical Measurements. The voltammetric experiments were performed with Autolab PGSTAT 20 and PSTAT 10 instruments (Eco-Chemie, Utrecht, The Netherlands) in conjunction with Metrohm VA 663 electrode stands (Metrohm, Switzerland) and a 486 personal computer. The electrochemical cell consisted of a three-electrode setup. The reference electrode was Ag/AgCl (saturated KCl with $E = 0.204$ V vs SHE), and the auxiliary electrode was a platinum wire. Electrodes used in this study were paraffin-impregnated graphite electrodes (PIGE) prepared from graphite rods (electrodes for spectrographic analysis, VEB Elektrokohle, Lichtenberg, Germany) impregnated in melted paraffin.[13,14] The sample preparation was carried out as follows: 1−3 mg of the sample powder was placed on a glass plate. The electrode was gently rubbed over the material in order to immobilize some compound at the electrode surface. After measurement, the electrode surface was cleaned with a razor blade. All electrolyte solutions were degassed with high-purity nitrogen for 10 min prior to the electrochemical measurements.

For the ring-disk experiment, a four-electrode potentiostat PG 287 (HEKA Elektronik, Lambrecht, Germany) with the following experimental setup was used: A conventional rotating disk electrode with the glassy carbon electrode replaced by a paraffin-impregnated graphite rod was used in conjunction with a platinum wire (∅ 0.5 mm) winded around the graphite electrode over a distance of approximately 1 mm. The ring electrode was in-plane with the disk electrode. The sample was immobilized at the graphite electrode as usual. This electrode could then be polarized to electrolyze the immobilized compound. At the platinum wire, a constant potential of −100 mV was applied in order to accumulate silver ions that were expelled from the solid. In the subsequent step, the accumulated silver was stripped off anodically.

Electrochemical Quartz Crystal Microbalance (ECQM) Measurements. ECQM measurements were performed using a μ-Autolab (Eco-Chemie, Utrecht, The Netherlands) combined with a Fluke PM6680B frequency counter (Fluke, The Netherlands) and a 10 MHz oscillator Model 230 with AT-cut gold coated plano-convex quartz crystals (Technical Department, Institut Chemii Fizycznej Polskiej Akademii Nauk, Poland).

Microscopic in Situ Diffuse Reflectance Spectroelectrochemical Measurements. A special electrochemical cell was used to perform electrochemical measurements with solid particles immobilized on the surface of graphite electrodes with in situ recording of diffuse reflectance spectra under an incident-light microscope. The microscope was a Leitz Laborlux 12 POL S incident-light microscope (Leica Mikroskopie und Systeme GmbH, Germany) with a 100 W halogen incandescent lamp. A 20-fold magnification was used for the spectroelectrochemical measurements. Two crossed linear polarizing filters minimized the specular reflectance. The spectrometer, which was coupled via fiber optics, was a transputer-integrated diode array system (TIDAS) (J&M Analytische Mess- und Regeltechnik GmbH, Ahlen, Germany) with a spectral range from 320 to 950 nm. It was interfaced to a Pentium personal computer.

The detailed description of the experimental setup is given in a previous work.[15]

Preparation. All chemical operations were carried out using bidistilled water and analytical or reagent grade chemicals. $K_4[Mo^{IV}(CN)_8]$ was synthesized by the procedure described by Furman et al.[16] Anal. Calcd: C, 19.33; N, 22.55; H, 0.80. Found: C, 18.81; N, 21.76; H, 0.85. $K_3[Mo^{V}(CN)_8]$ was obtained by oxidizing a solution of $K_4[Mo^{IV}(CN)_8]$ with manganate(VII). Potassium octacyanotungstate(IV) was produced by the procedure described by Brauer[17] Anal. Calcd: C, 16.96; N, 19.78; H, 0.35. Found: C, 16.91; N, 19.33; H, 0.30. This is in agreement with the monohydrate $K_4[W^{IV}(CN)_8]\cdot H_2O$.

Potassium hexacyanoferrate(II) and -(III) (Laborchemie Apolda, Germany) were used to precipitate the silver hexacyanoferrates.

A certain percentage of silver-ion sites in the lattice of silver octacyanomolybdate(IV) (Ag*ocm*(IV)) and silver hexacyanoferrate(II) (Ag*hcf*(II)) can be occupied by potassium ions. Depending on the desired content of alkali ions ($Ag_{4-x}K_x[Mo^{IV}(CN)_8]$ and $Ag_{4-x}K_x[Fe^{II}(CN)_6]$ with $0 < x < 1$), the following procedures have been applied:

Maximized K^+ Content (Procedure I). To obtain the composition $Ag_3K[X]$ ($X = [Mo(CN)_8]^{4-}$ and $[Fe(CN)_6]^{4-}$) stoichiometric amounts of 0.01 M silver nitrate solution were added dropwise to a stirred solution containing 0.01 M potassium octacyanomolybdate or hexacyanoferrate, respectively, dissolved in a saturated potassium nitrate solution. The precipitate was washed with a 1 M potassium nitrate solution and was then vacuum-dried.

Minimized K^+ Content (Procedure II). To precipitate the $Ag_4[X]$ compounds, an excess of silver nitrate solution was added to a solution of $K_4[Mo(CN)_8]$ or $K_4[Fe(CN)_6]$ dissolved in water. The precipitate was then allowed to age for 2 h in the presence of silver ions before being washed with distilled water.

The octacyanomolybdates of Cd^{2+}, Co^{2+}, Cr^{2+}, Cu^{2+}, Fe^{2+}, Mn^{2+}, Ni^{2+}, Pb^{2+}, and Zn^{2+} were precipitated by dropwise adding a 0.01 M metal nitrate solution to the 0.01 M solution of $K_4[Mo(CN)_8]$. $Cr_2[Mo(CN)_8]$ was precipitated under a nitrogen atmosphere to prevent the oxidation of chromium(II).

The elemental composition of the synthesized compounds was determined by CHN analysis and atomic absorption spectrometry. The following results were obtained for the silver compounds:

Silver octacyanomolybdate: precipitated following procedure I, $Ag_{3.36}K_{0.64}[Mo(CN)_8]$; precipitated following procedure II, $Ag_4[Mo(CN)_8]$. **Silver hexacyanoferrate:** precipitated following procedure I, $Ag_{3.05}K_{0.95}[Fe(CN)_6]$; precipitated following procedure II, $Ag_4[Fe(CN)_6]$.

Structural Chemistry of the Silver Octacyanometalates and Hexacyanoferrate. As is known for AgCN, silver(I) preferentially forms linear bonds to its neighbor atoms. Thus, the nearly perfect octahedral orientation of the cyanide ligands in the hexacyanoferrate ion is an ideal basis for a three-dimensional structure of the silver hexacyanoferrate lattice. The scaffold of silver hexacyanoferrate(II/III) is based on an $Ag_3[Fe(CN)_6]^{-/0}$ unit (Figure 1) with empty interstitials, in the case of the hexacyanoferrate(III), and K^+ or Ag^+ occupied interstitials, in the case of the hexacyanoferrate(II).[18] It possesses a hexagonal elementary cell with $a = 7.02$ Å and $c = 7.25$ Å. The C−N bond length is 1.12 Å, and the Fe−C bond length is 1.85 Å. In contrast to the hexacyanoferrate ion, the dodecahedral, or square

(14) Scholz, F.; Lange, B. *Trends Anal. Chem.* **1992**, *11*, 359.

(15) Schröder, U.; Scholz, F. *J. Solid State Electrochem.* **1997**, *1*, 62−67.

(16) Furman, N. H.; Miller, C. O. In *Inorganic Synthesis*; Audrieth, L.F., Ed.; McGraw−Hill: New York, 1950; Vol. III, p 160.

(17) Brauer, G. *Handbuch der Präparativen Anorganischen Chemie*; Enke: Stuttgart, 1954; p 1068.

(18) Kahlert, H. Ph.D. Thesis, Humboldt-Universität, Berlin, Germany, 1998.

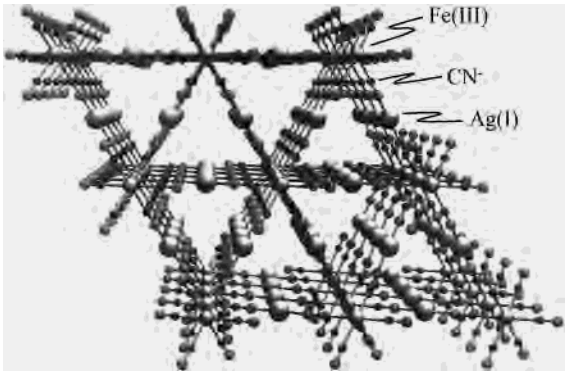

Figure 1. Structure of silver(I) hexacyanoferrate(III) along the [001] axis (reproduced with permission[18]).

antiprismatic, configurations of the octacyanometalate ions allow a crystalline lattice to be formed only with cations, which do not require a linear preferential orientation. Hence, only crystal data of the soluble alkali salts (e.g., $K_4[Mo(CN)_8]$[19] and $H_4[Mo(CN)_8]$[20] and the corresponding tungsten compounds) and the relatively sparingly soluble $Tl_4[Mo(CN)_8]$ can be found in the literature.[21] In the latter compound, which has been reported to consist of square antiprismatic anion polyhedra, the C−N−Tl bond angles vary between 83 and 164°.[21] This flexibility of the bond angles is a prerequisite for the good crystallinity of the compound.

Results and Discussion

The powder diffractograms of $Ag_3[Fe^{III}(CN)_6]$ and $Ag_3K[Fe^{II}(CN)_6]$ are given in Figure 2, parts a and b. They reflect that both compounds possess a very similar structure, despite the presence of potassium ions in the reduced compound. This indicates that the potassium ions are only weakly interacting with the cyanide ligands of the Ag*hcf*(II) (*hcf* ≡ hexacyanoferrate), and thus, they only slightly perturb the host scaffold, if at all.

When some micrograms of microcrystalline $Ag_3K[Fe^{II}(CN)_6]$ were mechanically immobilized on a gold-plated quartz crystal of an ECQM and immersed into a 0.1 M KNO_3 solution, an addition of silver nitrate (the resulting silver concentration was 10^{-3} M) decreased the frequency of the oscillator crystal by about 2000 Hz. Obviously, this is due to the increased mass of immobilized compound on the surface of the crystal. This mass increase is caused by the exchange of the incorporated potassium ions by silver ions according to the following reaction:

$$\{Ag_3K[Fe^{II}(CN)_6]\} + Ag^+ \rightarrow \{Ag_4[Fe^{II}(CN)_6]\} + K^+ \quad (1)$$

(Braces denote solid phases.)

This is a simple ion-exchange reaction known from literature.[22] The ion exchange is accompanied by very pronounced lattice alterations, that is, an amorphization, which can be seen from the powder diffraction pattern of the reaction product (cf. Figure 2c).

Electrochemical measurements (see below) show that the storage of $Ag_3K[Fe(CN)_6]$ in water causes the following conversion of one solid compound into another to occur:

$$4\{Ag_3K[Fe^{II}(CN)_6]\} \rightarrow 3\{Ag_4[Fe^{II}(CN)_6]\} + [Fe^{II}(CN)_6]^{4-} + 4K^+ \quad (2)$$

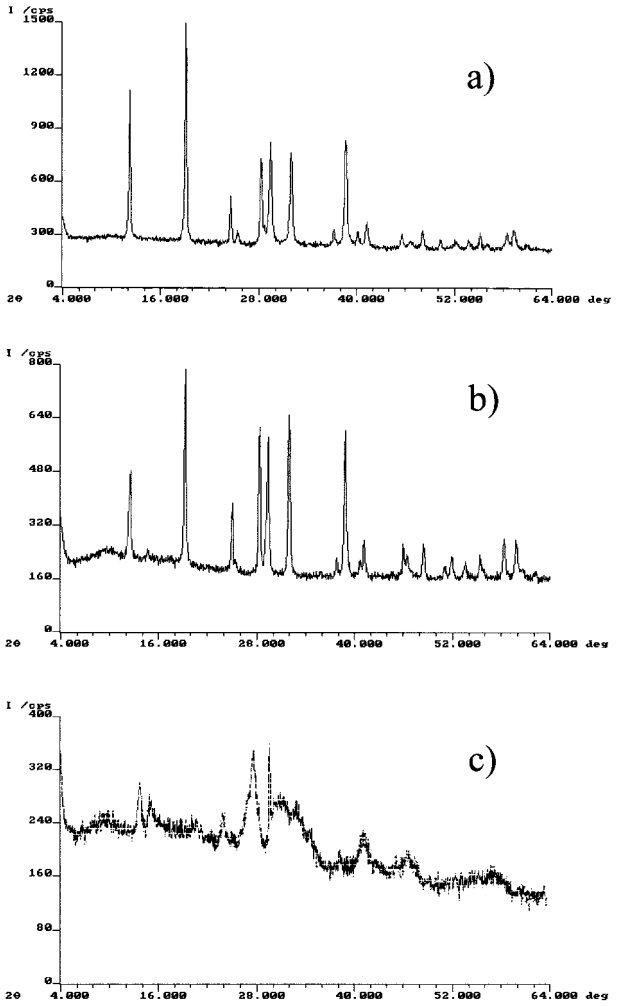

Figure 2. Powder diffraction patterns of (a) $Ag_3[Fe(CN)_6]$, (b) $Ag_3K[Fe(CN)_8]$, and (c) $Ag_4[Fe(CN)_6]$ obtained by storing $Ag_3K[Fe(CN)_8]$ in a 0.1 M $AgNO_3$ for 10 h.

Equations 1 and 2 can be understood on the basis of the solubility equilibria of $Ag_3K[Fe(CN)_6]$ and $Ag_4[Fe(CN)_6]$:

$$\{Ag_3K[Fe^{II}(CN)_6]\} \rightleftarrows [Fe^{II}(CN)_6]^{4-} + K^+ + 3Ag^+ \quad (K_L) \quad (3)$$

$$\{Ag_4[Fe^{II}(CN)_6]\} \rightleftarrows [Fe^{II}(CN)_6]^{4-} + 4\,Ag^+ \quad (K_L') \quad (4)$$

with $K_L = 2.1 \cdot 10^{-9}$mol/L and $K_L' = 3.3 \cdot 10^{-5}$mol/L.[23,24] In the case of $Ag_4[Fe(CN)_6]$, these solubility products are the result of a strong, partially covalent interaction of the extra silver ions with the cyanide ligands.[25,26] In the case of $Ag_3K[Fe(CN)_6]$, they are the result of comparably weak, mainly electrostatic bonding of the potassium ions . Later, it will be shown that similar reprecipitation reactions also occur with silver and all metal(II) octacyanomolybdates, octacyanotungstates, and

(19) König, E. *Z. Naturforsch.* **1968**, *23a*, 853−860.
(20) Basson, S. S.; Bok, L. D. C.; Leipoldt, J. G. *Acta Crystallogr.* **1970**, *B26*, 1209.
(21) Meske, W.; Babel, D. *J. Alloys Compd.* **1992**, *183*, 158−167.
(22) (a) Tananaev, I. V.; Kachukhashvili, S. I. *Zh. Neorg. Khim.* **1962**, *7*, 1516−1520; Tananaev, I. V.; Kachukhashvili, S. I. *Russ. J. Inorg. Chem.* **1962**, *7*, 782−785. b) Tananaev, I. V.; Levina, I. M. *Zh. Neorg. Khim.* **1957**, *2*, 576−585.
(23) Zasepa, W. *Rocz. Chem.* **1968**, *42*, 1129−1135.
(24) Bellomo, A. *Talanta* **1970**, *17*, 1109−1114.
(25) Kerler, W.; Neuwirth, W., Fluck E. *Z. Phys.* **1963**, *175*, 200−220.
(26) Nekrasov, B. V.; Seifer, G. B.; Kharitonov, Yu. Ya. *Bull. Akad. Sci. USSR Div. Chem. Sci.* **1970**, 219−224.

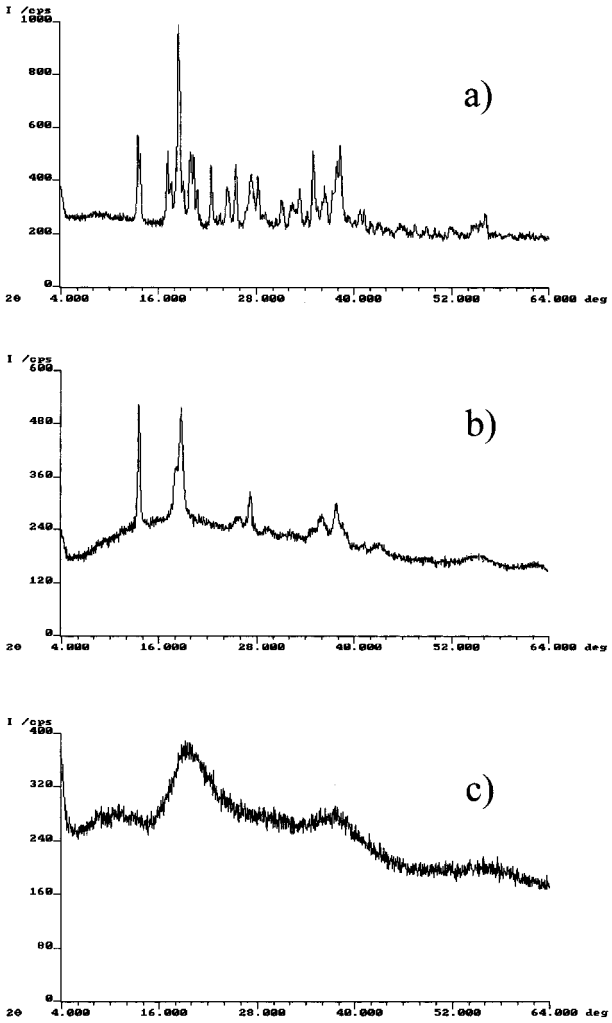

Figure 3. Powder diffraction pattern of (a) $Ag_3[Mo^V(CN)_8]$, (b) $Ag_4[Mo^{IV}(CN)_8]$, and of (c) $Ag_3[Mo^V(CN)_8]$ treated in a ball mill.

copper hexacyanoferrate. It is highly probable that these reactions also occur with all other sparingly soluble metal hexacyanoferrates, although this might not be easily detectable due to the special relation of the solubility products to each other.

Thus, eq 2 can be generalized for the silver salts as follows:

$$\begin{array}{ccc} 4\{Ag_3K[X]\} & \underset{+4K^+ + [X]^{4-}}{\overset{-4K^+ - [X]^{4-}}{\rightleftharpoons}} & 3\{Ag_4[X]\} \\ \Big\| & & \Big\| \\ 4[X]^{4-} + 4K^+ + 12Ag^+ & \underset{+4K^+ + [X]^{4-}}{\overset{-4K^+ - [X]^{4-}}{\rightleftharpoons}} & 12Ag^+ + 3[X]^{4-} \end{array} \quad (5)$$

where X represents $Fe^{II}(CN)_6$, $Mo^{IV}(CN)_8$, or $W^{IV}(CN)_8$.

Depending on the activity of K^+ and Ag^+ in the solution, the equilibrium will be shifted to either the left or the right side. It should be mentioned that the actual extent of these reactions will be strongly influenced by their kinetics. Although potassium ions are immediately exchanged by silver ions (as found from the quartz crystal microbalance experiment), the exchange of Ag^+ by K^+ is overtly slow.

The powder diffraction pattern of Ag*ocm*(V) (*ocm* ≡ octacyanomolybdate) and Ag*ocm*(IV) are shown in Figure 3, parts a and b. They reveal that both $Ag_4[Mo^{IV}(CN)_8]$ and $Ag_3[Mo^V(CN)_8]$ are characterized by a considerably high content of amorphous material, and a poor crystallinity in the case of Ag*ocm*(IV). The latter is caused by the extremely low solubility and the relative rigidity of the bond angle of the silver(I) ions.

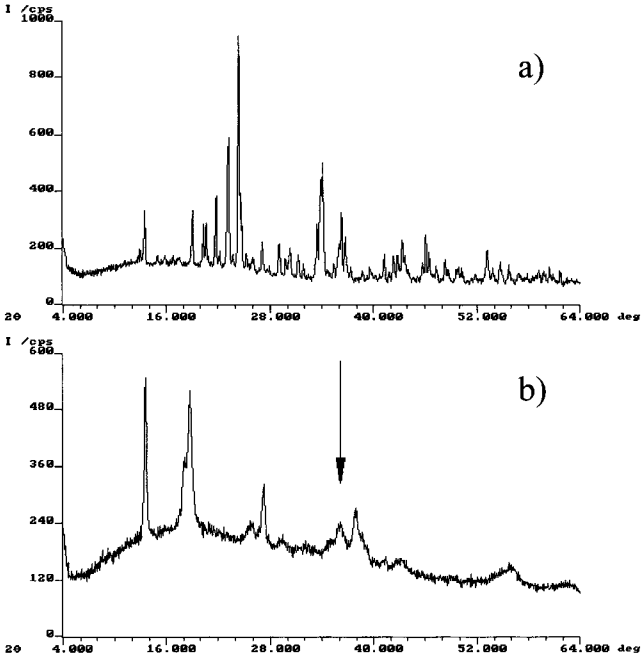

Figure 4. Powder diffraction pattern of the conversion of (a) $Tl_4[Mo^{IV}(CN)_8]$ to (b) $Ag_4[Mo^{IV}(CN)_8]$. The spectra have been recorded before (a) and after an overnight storage of $Tl_4[Mo^{IV}(CN)_8]$ in 0.1 M $AgNO_3$ solution.

In Figure 4, the powder diffraction patterns of thallium octacyanomolybdate(IV) before (Figure 4a) and after (Figure 4b) an overnight storage in silver nitrate solution are shown. The product of the overnight storage can be identified as $Ag_4[Mo(CN)_8]$. The conversion of the thallium to the silver compound, according to the following equation,

$$\{Tl_4[Mo^{IV}(CN)_8]\} + 4Ag^+ \rightarrow \{Ag_4[Mo^{IV}(CN)_8]\} + 4Tl^+ \quad (6)$$

is brought about by the much lower solubility of $Ag_4[Mo(CN)_8]$. This reaction provokes a dramatic decrease of crystallinity of the solid material. This deterioration of the long-range order can be understood to be a result of the rigid bond angle of the silver ions, in contrast to the flexible bonding between the thallium ions and the cyanide polyhedra. It was found that the powder diffraction patterns of silver octacyanomolybdate and silver octacyanotungstate (Ag*oct*) are nearly identical for the oxidized and the reduced compounds, respectively. This explains the strong similarities of the chemical and electrochemical properties.

As in the case of the Ag*hcf*(II) lattice, potassium ions can be incorporated into the lattice of Ag*oct*(IV) and Ag*ocm*(IV) (see the results of analysis). Unlike silver hexacyanoferrate(II), Ag*ocm*(IV) can only be produced with a maximum content of 0.64 K^+, that is, $Ag_{3.36}K_{0.64}[Mo^{IV}(CN)_8]$ when precipitated from a saturated potassium nitrate solution. As shown later, this formula describes the net composition of a mixture of $Ag_4[Mo(CN)_8]$ and $Ag_3K[Mo(CN)_8]$. Because of the ratio of the solubility products of these two compounds, it is probably impossible to achieve a higher potassium net content. Although only three of the four silver ions of Ag*hcf*(II) are part of the lattice framework, and therefore, the fourth (interstitial) ion can be replaced by a potassium ion without a dramatic loss of stability (the solubility of $Ag_4[Fe^{II}(CN)_6]$ and $Ag_3[Fe^{III}(CN)_6]$ are nearly equal), it takes four cations to connect the cyanide ligands of the octacyanomolybdate polyhedra. Replacing a silver

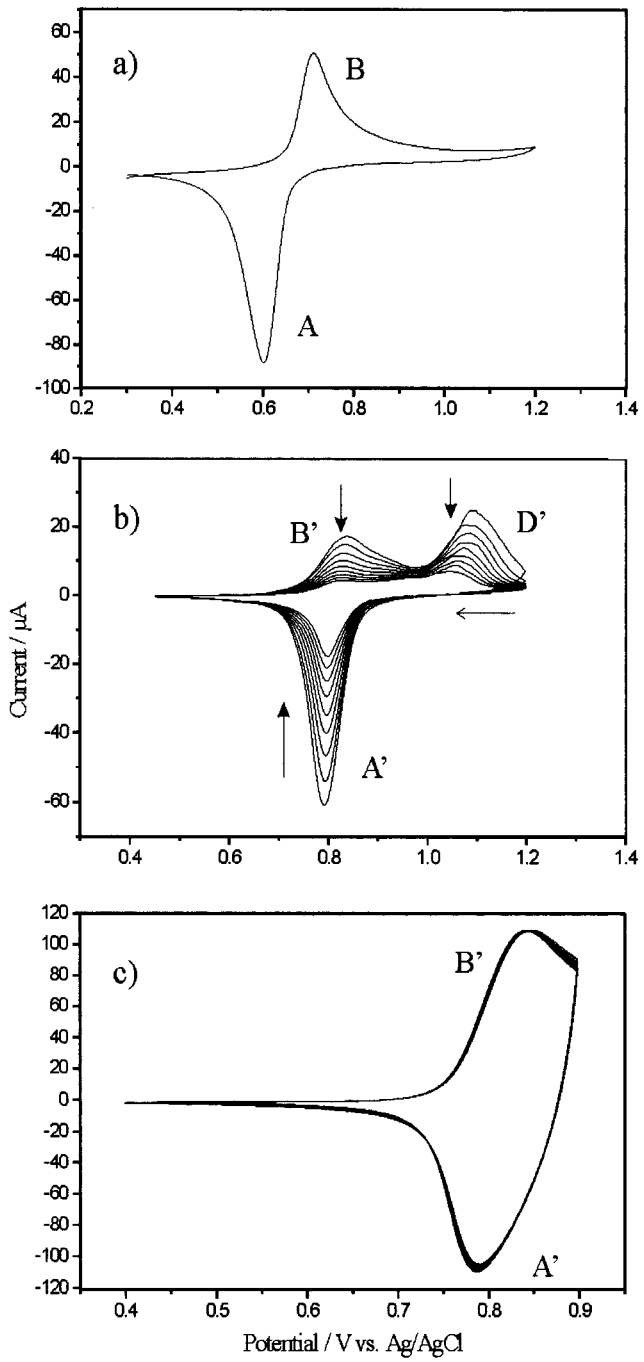

Figure 5. Cyclic voltammograms of (a) $Ag_3[Fe(CN)_6]$ and (b, c) $Ag_3[Mo^V(CN)_8]$ mechanically attached on the surface of a paraffin-impregnated graphite electrode and immersed in a 0.1 M KNO_3, scan rate 5 mV/s.

ion with a potassium ion thereby weakens the lattice structure and raises the solubility of the compound.

The Electrochemistry of Ag*hcf* and Ag*ocm* in Potassium Nitrate Electrolyte. Along with the structures, the electrochemical properties of octacyanotungstates and octacyanomolybdates are very similar. Therefore, it suffices to explain the electrochemical behavior using the example of silver octacyanomolybdate. Cases in which differences are observed will be noted.

The voltammetry of solid Ag*hcf*(II/III) or Ag*ocm*(IV/V), immobilized on the electrode surface and adjacent to a potassium nitrate solution, is strongly affected by the precipitation equilibria presented in eq 5. Figure 5 shows the very different electrochemical behaviors of $Ag_3[Fe^{III}(CN)_6]$ and $Ag_3[Mo^V(CN)_8]$ under these conditions. The voltammetry of Ag*hcf*(III) (Figure 5a) is chemically reversible. It is characterized by the signal pair of A and B. The dependence of the formal potential, $E_{f_{A/B}}$, on the activity of the potassium ions in the electrolyte solution, that is, $\Delta E_{f_{A/B}}/\Delta \log a_{K^+} = 60.5$ mV, indicates the following reaction:

$$\{Ag_3[Fe^{III}(CN)_6]\} + K^+ + e^- \underset{B}{\overset{A}{\rightleftharpoons}} \{Ag_3K[Fe^{II}(CN)_6]\} \quad (7)$$

An additional oxidation peak occurs at about 1100 mV in the cyclic voltammogram of the analogue molybdenum compound (D′, Figure 5b), which is in contrast to the results found for hexacyanoferrate. With the help of a modified ring-disk experiment that was carried out in a 1 M KNO_3 solution, and which is described in detail in the Experimental Section, the origin of this peak could be revealed. While the rotating graphite electrode, which was previously modified with a sample having a net composition of $Ag_{3.6}K_{0.4}[Mo^{IV}(CN)_8]$, was polarized toward positive potential, the surrounding platinum wire was held at a constant potential of −100 mV in order to trap silver expelled from the solid during the oxidation. This experiment showed that only the oxidation process D′ is accompanied by the expulsion of silver ions into the electrolyte solution. The presence of the peak D′ is also accompanied by a fast decrease of the voltammetric signals. Restricting the oxidation sweep to a limit of 900 mV results in a stable and chemically reversible electrochemistry (Figure 5c) with the dependence $\Delta E_f/\Delta \log a_{K^+} = 59.5$ mV. From this, it follows that the redox process, analogous to reaction 7, is based upon the following reaction:

$$\{Ag_3[Mo^V(CN)_8]\} + K^+ + e^- \underset{B'}{\overset{A'}{\rightleftharpoons}} \{Ag_3K[Mo^{IV}(CN)_8]\} \quad (8)$$

Figure 6 shows the cyclic voltammograms of $Ag_4[Fe^{II}(CN)_6]$ (Figure 6a) and $Ag_4[Mo^{IV}(CN)_8]$ (Figure 6b), which were recorded in the presence of a 0.1 M KNO_3 electrolyte. In the first cycle, both figures exhibit the same characteristics. During the first oxidation half-scan, the compounds are oxidized, accompanied by a loss of silver ions:

$$\{Ag_4[X]\} \rightarrow \{Ag_3[X]\} + Ag^+ + e^- \quad (9)$$

The expelled silver ions escape by diffusion into the bulk solution, and hence, they cannot be completely reinserted into the compound during the next reduction. Instead of Ag^+, K^+ is inserted during the subsequent reduction:

$$\{Ag_3[X]\} + K^+ + e^- \rightarrow \{Ag_3K[X]\} \quad (10)$$

At this point, the differences between Ag*ocm*(IV) and Ag*hcf*(II) become very obvious: Although Ag*hcf*(II) is able to form $Ag_3K[Fe(CN)_6]$, which is stable when in contact with a 0.1 M KNO_3 solution, the position of the precipitation equilibrium (5) of Ag*ocm*(II) leads to an internal reconstruction under partial re-formation of $Ag_4[Mo(CN)_8]$:

$$\{Ag_4[Mo^{IV}(CN)_8]\} \xrightarrow{-Ag^+ - e^-} \{Ag_3[Mo^V(CN)_8]\} \underset{-nK^+ - \frac{1}{4}[Mo(CN)_8]^{4-}}{\overset{+K^+ + e^-}{\rightleftharpoons}} \{Ag_3K[Mo^{IV}(CN)_8]\} \quad (11)$$

The result of this reaction is a mixture of the two compounds $Ag_4[Mo(CN)_8]$ and $Ag_3K[Mo(CN)_8]$. Instead of giving the ratio of these two compounds, one can write the following formula: $Ag_{3.36}K_{0.64}[Mo^{IV}(CN)_8]$. The oxidation of these two compounds occurs at well-separated potentials, as it comprises the oxidation

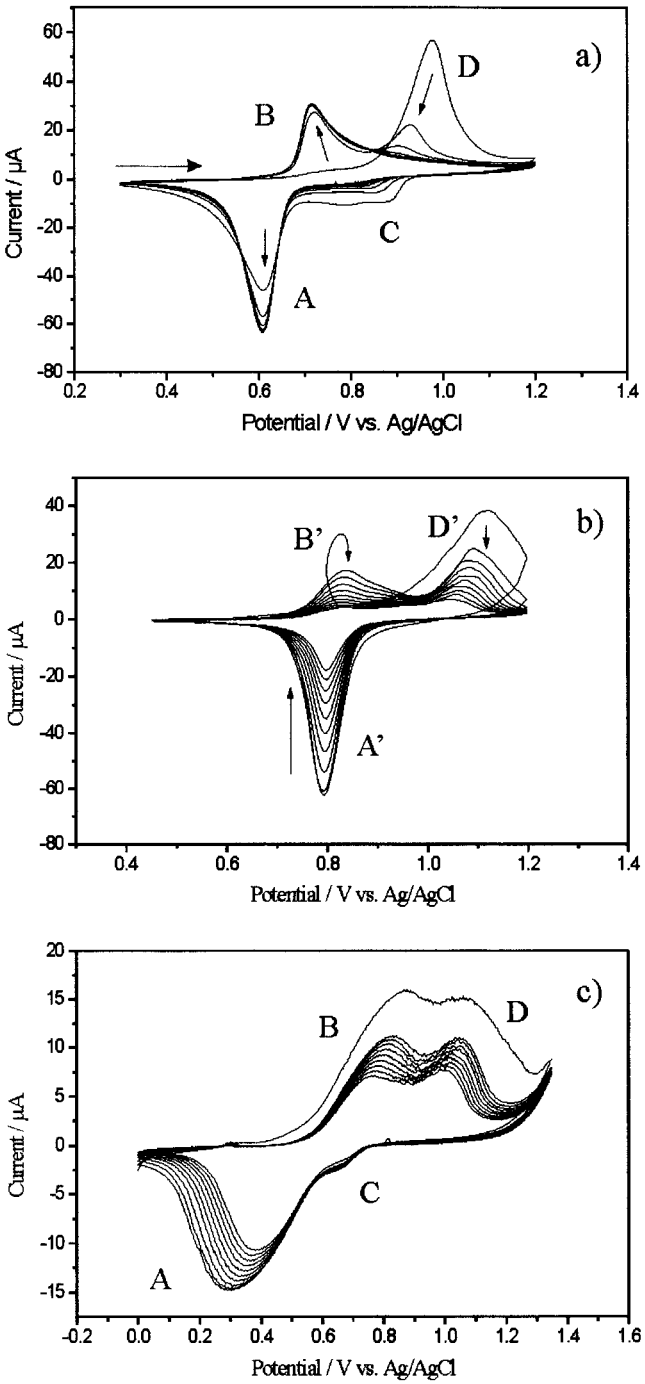

Figure 6. Cyclic voltammograms of (a) $Ag_4[Fe(CN)_6]$ and (b) $Ag_4[Mo(CN)_8]$ recorded in the presence of 0.1 M KNO_3 electrolyte solution and of (c) $Ag_3K[Fe(CN)_6]$ in the presence of 10^{-3}M KNO_3, scan rate 5 mV/s.

of two differently coordinated octacyanomolybdate ions. Furthermore, the two distinct oxidation signals unambiguously prove that no mixed crystals have formed between $Ag_3K[Mo^{IV}(CN)_8]$ and $Ag_4[Mo^{IV}(CN)_8]$. In that case, according to mixed phase thermodynamics, and in accordance with experimental results,[27−29] one would observe a single signal shifting from the position of one compound to the position of the other. Here, the difference between the bonding of the inserted K^+ and the Ag^+ plays a crucial role. The potassium ions are only electrostatically bonded, whereas the silver ions are partially covalently bonded. The silver ions reduce the electron density of the redox active central atom (e.g., of the 3d orbital of the iron(II) in the hexacyanoferrate[25]) leading to a shift of the redox potential toward more positive values, as shown in Table 1. Table 1 also includes data for the Tl^+ insertion electrochemistry. The potential shift turns out to be nearly constant (about 300 mV) for all investigated compounds. This influence of the metal ions coordinated to the complex ion (*hcf*, *ocm*, *oct*) has already been studied in detail in case of metal hexacyanoferrates.[30]

Table 1. Formal Potentials E_f [mV vs Sat. Ag/AgCl] Determined by Cyclic Voltammetry as $E_f = (E_{pc} + E_{Pa})/2$

	0.1 M KNO_3	0.1 M $TlNO_3$	0.1 M $AgNO_3$
$Ag_3[Mo(CN)_8]$	831.2 ± 0.8	948.3 ± 5.0	1145.4 ± 4.8
$Ag_3[W(CN)_8]$	574.4 ± 3.4	663.5 ± 4.5	871.6 ± 3.0
$Ag_3[Fe(CN)_6]$	671.0 ± 4.0	788.6 ±3.2	1007.4 ± 4.8

The process of continuous re-formation and dissolution finally leads to a total degradation of the solid material at the electrode surface and a disappearance of the voltammetric response.

As expected, the same situation arises for Ag*hcf*(II/III) for cases in which the potassium ion concentration in the electrolyte solution is lower than 10^{-2} mol·L^{-1} (Figure 6c):

$$\{Ag_4[Fe^{II}(CN)_6]\} \xrightarrow{-Ag^+ -e^-} \{Ag_3[Fe^{III}(CN)_6]\} \underset{-nK^+ - \frac{1}{3}[Fe(CN)_6]^{4-}}{\overset{+K^+ +e^-}{\rightleftharpoons}} \{Ag_3K[Fe^{II}(CN)_6]\} \quad (12)$$

Figure 7, parts a and b, show that copper hexacyanoferrate(II) exhibits a similar behavior. Two distinct oxidation signals can be observed which are based upon the following redox processes (13, 14).

$$2\{Cu_2[Fe^{II}(CN)_6]\} \rightleftarrows 2\{Cu_{1.5}[Fe^{III}(CN)_6]\} + Cu^{2+} + 2e^- \quad (13)$$

$$\{Cu_{1.5}K[Fe^{II}(CN)_6]\} \rightleftarrows \{Cu_{1.5}[Fe^{III}(CN)_6]\} + K^+ + e^- \quad (14)$$

Both reactions are chemically reversible in 0.1 M solutions of the respective cation.

Electrochemical Determination of the Potassium Content of Solid Cyanides. The phenomenon that the release of two different interstitial cations during oxidation prompts the occurrence of two different voltammetric signals can be used for the quantitative evaluation of the composition of silver octacyanomolybdates. As outlined in Figure 8, parts a and b, it is based upon a two-step chronocoulometric oxidation of samples with a net composition $Ag_{4-x}K_x[Mo^{IV}(CN)_8]$.

The sample was immobilized on the surface of a paraffin-impregnated graphite electrode, which was then immersed into a potassium nitrate solution. To minimize the reprecipitation reaction (5), a relatively concentrated (1 mol·L^{-1}) potassium nitrate solution was used. In the first step, the electrode was polarized toward a potential at which the oxidation of $Ag_3K[Mo^{IV}(CN)_8]$ proceeds accompanied by the release of potassium ions (see Figure 8a). The potential was held at this value for 250 s in order to allow a complete conversion of the sample. The second potential step was aimed to oxidize $Ag_4[Mo^{IV}(CN)_8]$ accompanied by the release of silver ions.

The results of the chronocoulometric determination of the composition of differently precipitated silver octacyanomolyb-

(27) Bond, A. M.; Scholz, F. *Langmuir* **1991**, *7*, 3197−3204.
(28) Reddy, S. J.; Dostal, A.; Scholz, F. *J. Electroanal. Chem.* **1996**, *403*, 209−212.
(29) Meyer, B.; Zhang, S.; Scholz, F. *Fresenius' J. Anal. Chem.* **1996**, *68*, 6, 267−270.
(30) Scholz, F.; Dostal, A. *Angew. Chem.* **1995**, *107*, 2876−2878 (Scholz, F.; Dostal, A. *Angew. Chem., Int. Ed. Engl.* **1995**, *34*, 2685−2687).

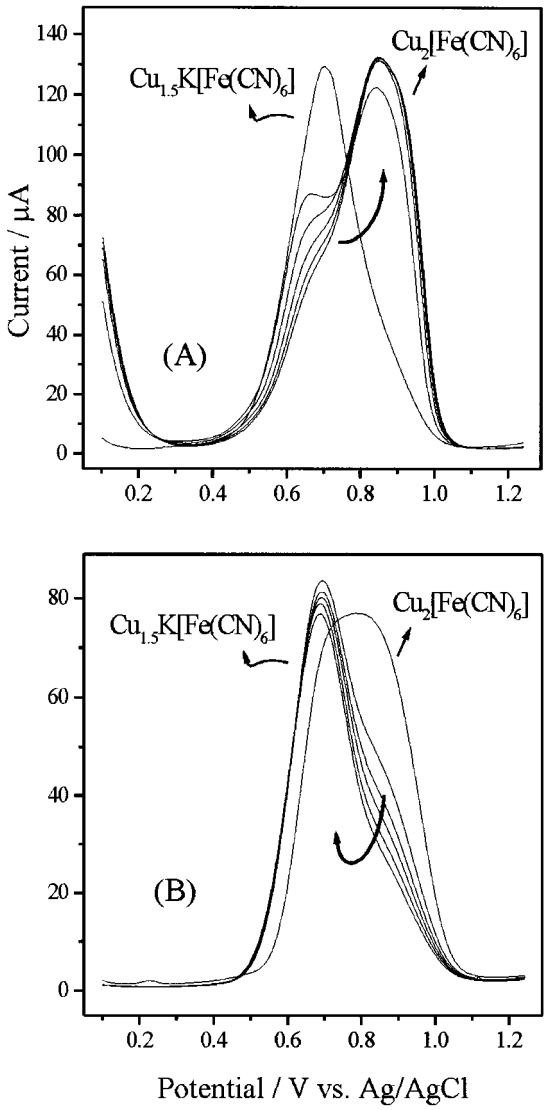

Figure 7. Succeeding differential pulse voltammograms of the oxidation of a sample of $Cu_{1.5}K[Fe(CN)_6]$ immobilized on the surface of a paraffin-impregnated graphite electrode and immersed in a 0.2 M $Cu(NO_3)_2$ solution (A). The compound was rereduced at 200 mV after each scan. After twenty redox cycles, the electrode was immersed in a 0.1 M KNO_3 solution and differential pulse voltammograms of the oxidation (B) were recorded as described for A. (Step potential = 5 mV, modulation amplitude = 25 mV.)

dates, with a net composition $Ag_{4-x}K_x[Mo^{IV}(CN)_8]$, are in good agreement with the data obtained by atomic absorption spectrometry (AAS). For the calculation, it was assumed that the unit $\{Ag_3[Mo(CN)_8]^-\}$ remains unchanged. On the basis of the formula $Ag_{1-x}K_x\{Ag_3[Mo(CN)_8]\}$, the ratio Ag^+/K^+ was calculated following $Q_{Ag+} + Q_{K+} = 1$, where Q is the charge of the single-oxidation processes normalized to the total oxidation charge.

The net composition of two different samples of $Ag_{4-x}K_x[Mo^{IV}(CN)_8]$ is determined by:

AAS	chronocoulometry
$Ag_{3.36}K_{0.64}[Mo(CN)_8]$	$Ag_{3.41}K_{0.59}[Mo(CN)_8]$
$Ag_{3.78}K_{0.22}[Mo(CN)_8]$	$Ag_{3.77}K_{0.23}[Mo(CN)_8]$

The outlined approach can probably be applied to other complex cyanides as well.

The Electrochemistry of Silver Octacyanomolybdate in the Presence of Silver Nitrate Electrolyte. Equation 15 depicts

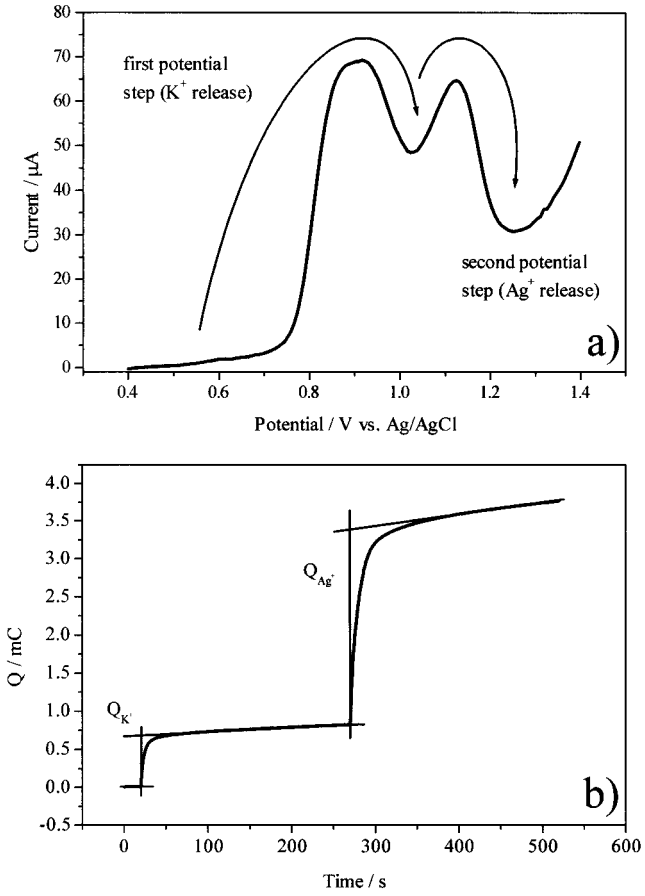

Figure 8. (a) Linear sweep voltammogram (scan rate 10 mVs^{-1}) of the oxidation of $Ag_{3.36}K_{0.64}[Mo(CN)_8]$ in the presence of 1 M KNO_3 solution. (b) chronocoulometric plot of the oxidation of a $Ag_{4-x}K_x[Mo(CN)_8]$; Initial potential: 0.6 V, first potential step: 1.05 V, second potential step: 1.25 V.

the single-electron/single-ion transfer reaction that is expected for the reaction of silver octacyanomolybdate in the presence of a silver nitrate solution.

$$\{Ag_4[Mo^{IV}(CN)_8]\} \rightleftarrows \{Ag_3[Mo^{V}(CN)_8]\} + Ag^+ + e^- \quad (15)$$

For this simple reaction, a single voltammetric system can be expected. Figure 9 shows that the reality is more complex. It can be seen that, depending on the scan rate, two main signal systems appear (A_{ox}/A_{red} and B_{ox}/B_{red}). Additionally, the peaks of the system B_{ox}/B_{red} are split. A similar peak splitting can be observed in the voltammogram of silver hexacyanoferrate (Figure 10).

The peaks of the systems A_{ox}/A_{red} and B_{ox}/B_{red} (Figure 9) differ in their half width, peak separation, and scan rate behavior. In Figure 11 a, the result of an ECQM measurement is presented. It shows that the reduction of $Ag_3[Mo^{V}(CN)_8]$ is accompanied by a decrease in the oscillation frequency, indicating an increase in the mass of the immobilized compound. The subsequent oxidation proceeds with a decrease in mass, indicating a release of cations. The shape of the derivative of the frequency change and the corresponding cyclic voltammogram (cf. Figure 11b) are quite similar, proving that the mass-to-charge ratio remains constant during the potential sweep. This supports the assumption that only one cation is involved in the different peaks. These results, and the dependence of the formal potentials of both redox systems on the silver ion activity, that is, $\Delta E_{f_{Aox/Ared}}/\Delta \lg a_{Ag^+} = 55$ mV and $\Delta E_{f_{Box/Bred}}/\Delta \lg a_{Ag^+} = 53.3$ mV, indicate

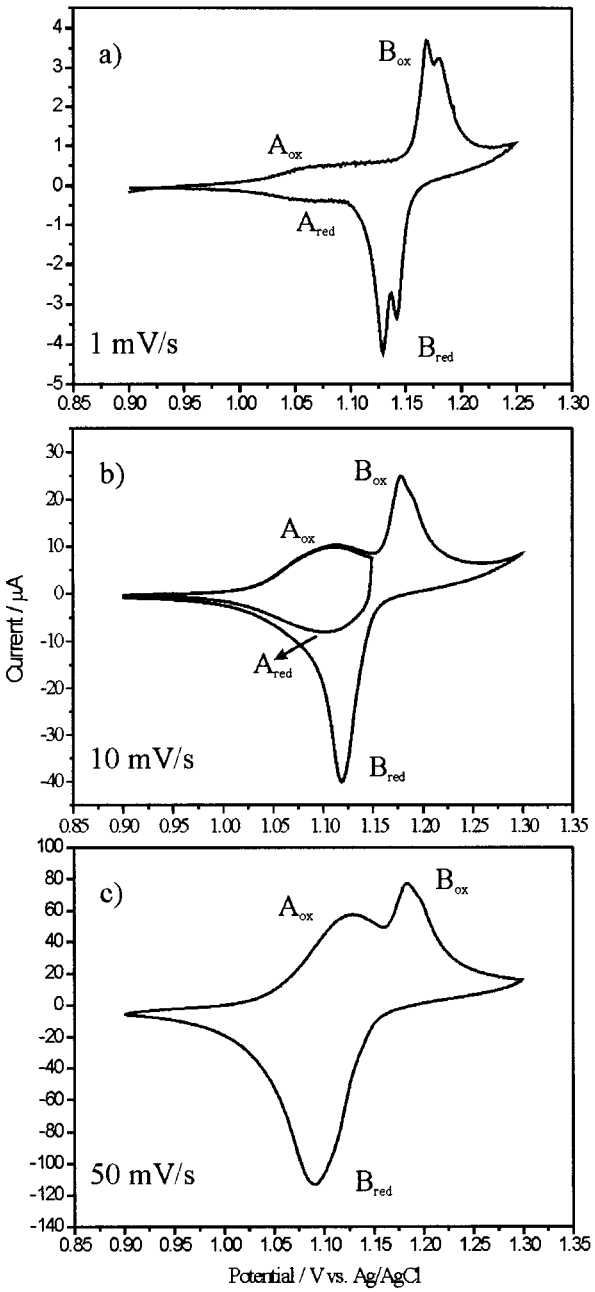

Figure 9. Cyclic voltammograms of a sample of $Ag_3[Mo(CN)_8]$ immobilized on the surface of a paraffin-impregnated graphite electrode and immersed in a 0.1 M $AgNO_3$ solution.

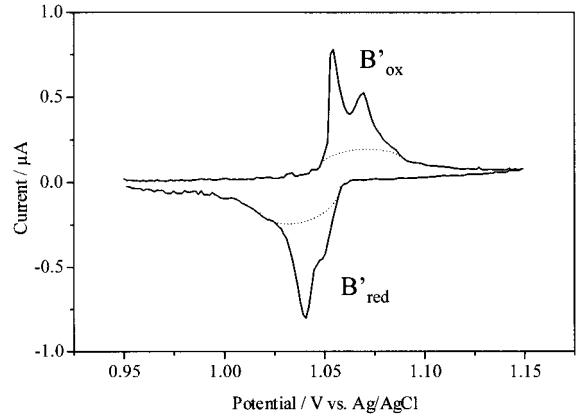

Figure 10. Cyclic voltammogram of a sample of $Ag_3[Fe(CN)_6]$ immobilized on the surface of a paraffin-impregnated graphite electrode and immersed in a 0.1 M $AgNO_3$ solution, scan rate 0.1 mV/s.

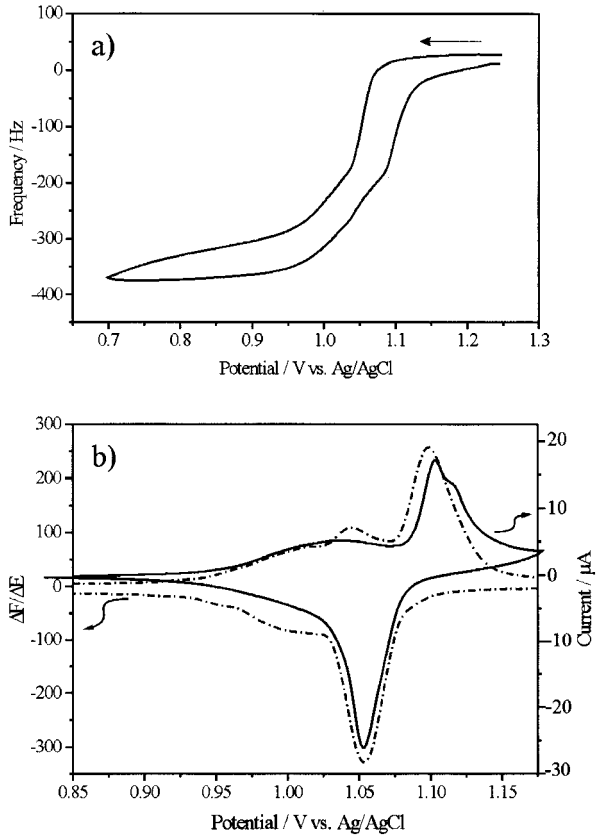

Figure 11. (a) Frequency response for the reduction and reoxidation of $Ag_3[Mo(CN)_8]$ deposited onto a 5 mm diameter gold-coated quartz crystal oscillator; 0.1 M $AgNO_3$, 5 mV/s. (b) Derivative of the frequency over the potential (dashed line) in comparison to a corresponding cyclic voltammogram.

that both of the signal systems are based on reaction 15. To elucidate the differences between the systems A_{ox}/A_{red} and B_{ox}/B_{red}, a variation of the scan rate was helpful. Figure 12a depicts these dependencies for the oxidation peaks A_{ox} and B_{ox}. With $i \propto v^1$, peak A_{ox} obeys a typical thin-layer behavior, whereas B_{ox} exhibits a diffusion control, that is, $i \propto v^{1/2}$.

Another important feature of the two systems is their reversibility. A_{ox}/A_{red} was found to be electrochemically reversible, having a zero-peak separation at scan rates lower than 0.5 mV/s. The considerable peak separation of B_{ox}/B_{red} (45 mV at a scan rate of 0.1 mV/s) indicates a kinetic control. The different reversibility can also be deduced from multistep chronocoulometric experiments. To study the redox systems under equilibrium conditions, A*gocm*(IV) was oxidized stepwise (the potential step was 10 mV, and the step time was 300 s), and the chronocoulograms were recorded. Figure 12b shows the results of this experiment in the form of a plot of the logarithm of the molar ratio C_{ox}/C_{red} versus potential. The C_{ox}/C_{red} ratio was calculated from the integrated charge related to the total oxidation charge. According to this plot, the system A_{ox}/A_{red} follows the Nernst equation for a one-electron process (with a slope of 1/59 mV). However, the system B_{ox}/B_{red} has a slope of 1/23 mV. The latter figure points to a very sudden conversion of the reduced form to the oxidized form and vice versa. This is also obvious from the cyclic voltammogram (Figure 9a), which shows very steep peaks of the system B_{ox}/B_{red}. This sudden conversion, exhibiting a super-Nerstian slope, may be caused by a nucleation and growth rate control. Nucleation

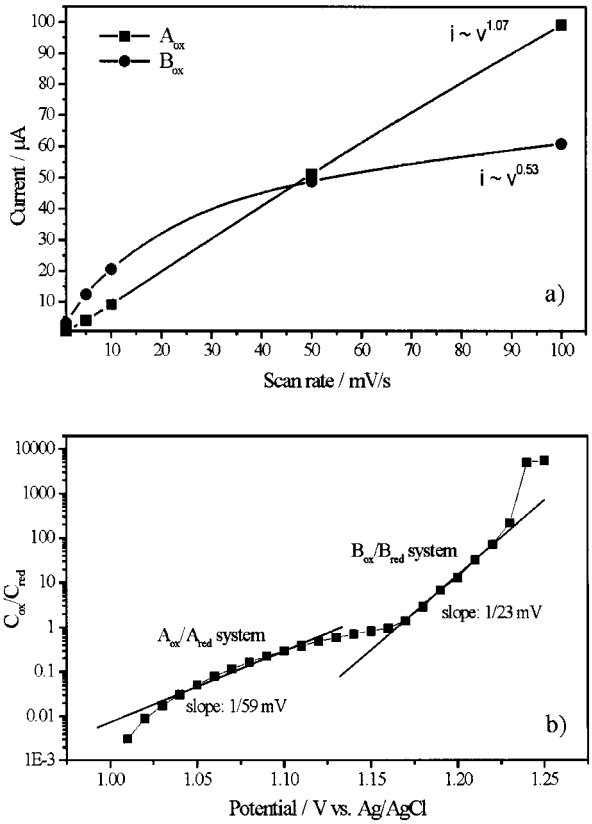

Figure 12. (a) Scan rate dependence of the oxidation peaks (see Figure 10a) of $Ag_3[Mo(CN)_8]$/electrolyte solution: 0.1 M $AgNO_3$. (b) Plot of the ratio of the molar ratios of the oxidized compound ($Ag_3[Mo(CN)_8]$) to the reduced compound ($Ag_4[Mo(CN)_8]$) derived from a multistep chronocoulometric experiment of the oxidation of $Ag_4[Mo(CN)_8]$/electrolyte solution: 0.1 M $AgNO_3$.

overpotential may exist, and surpassing it will lead to a very rapid conversion of the compound, limited only by the diffusion of cations in the solid phase (cf. last paragraph).

Summarizing these results and taking the poor crystallinity and high content of amorphous compound into consideration (cf. Figure 3), the following conclusions can be made. At the redox system A_{ox}/A_{red}, the conversion of amorphous particles takes place. The conversion of amorphous material proceeds very easily as the redox centers are better accessible; the cation transport is less hindered and less energy is necessary to reconstruct the lattice of these extremely small particles. This explains the high electrochemical reversibility of this redox process. On the other hand, the peak system B_{ox}/B_{red}, is caused by the electrolysis of larger particles of much better crystallinity. To prove this hypothesis, the raw material was milled in a ball mill until it became almost X-ray amorphous. The effect of this treatment on the crystallinity can be seen in Figure 3c. All of the sharp reflections of the powder diffraction pattern are eliminated, and only weak and broad signals remain, thus indicating a pronounced defect in structure and large amounts of amorphous compound. In the cyclic voltammogram of this sample, of $Ag_3[Mo^V(CN)_8]$, the sharp voltammetric signals (B_{ox}/B_{red}) are absent, and only a rather broad system is present. The same results were obtained from a milled sample of $Ag_4[Mo^{IV}(CN)_8]$.

This designation of the systems A_{ox}/A_{red} and B_{ox}/B_{red} is supported by spectroelectrochemical measurements. The diffuse reflectance spectra of Ag*ocm*(IV) (which is a yellow compound) and Ag*ocm*(V) (which is a dark brown compound)[15,31] were simultaneously measured during the cyclic voltammetry. The

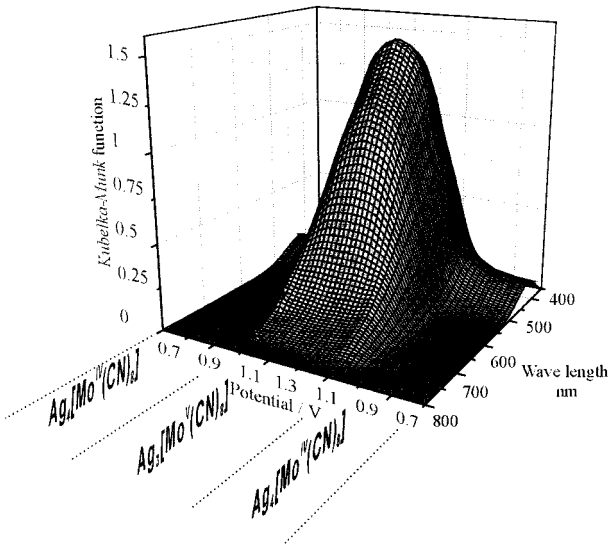

Figure 13. Kubelka−Munk function of Ag*ocm*(IV) immobilized on the surface of a paraffin-impregnated graphite electrode and immersed in a 0.1 M $AgNO_3$ solution. The Kubelka−Munk function was recorded in situ during the cyclic oxidation and rereduction of the compound.

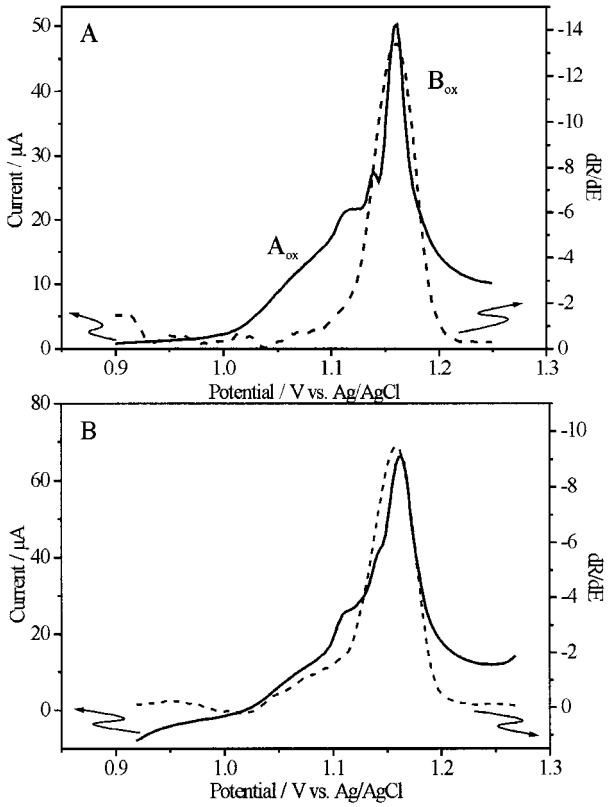

Figure 14. Linear sweep voltammogram (full line) of Ag*ocm*(IV/V) in the presence of 0.1 M $AgNO_3$, scan rate 1 mV/s. First derivative of the reflectance over the d*R*/d*E* potential (dotted line) versus potential. (A) The reflectance was measured for a sample layer of ~1 μm thickness. (B) The reflectance was measured for a sample layer of ~10 μm thickness.

changes of the Kubelka−Munk functions during a cyclic oxidation and rereduction are presented in Figure 13. For the two differently thick layers, a comparison was made between the voltammetric response and the first derivative of the reflectance over potential, that is, d*R*/d*E*. In the case of a thin

(31) Schröder, U.; Meyer, B., Scholz F. *Fresenius' J. Anal. Chem.* **1996**, *68*, 295−298.

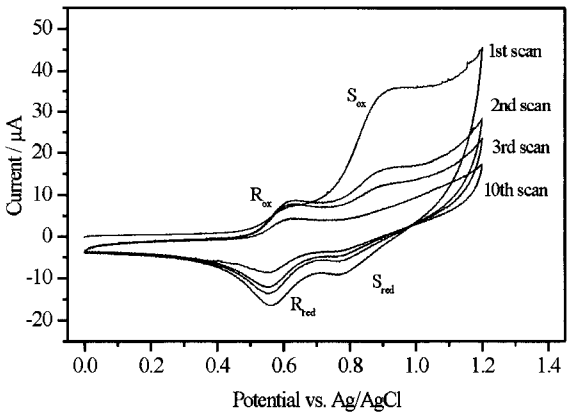

Figure 15. Cyclic voltammograms of $Co_2[Mo^{IV}(CN)_8]$ mechanically attached on the surface of a paraffin-impregnated graphite electrode and immersed in a 0.1 M KNO_3, scan rate 50 mV/s.

Table 2. Formal Potentials E_f [mV vs Sat. Ag/AgCl] of the Redox Systems of Octacyanomolybdates of Selected Bivalent Cations in the Presence of 0.1 M KNO_3 Determined by Cyclic Voltammetry as $E_f = (E_{pc} + E_{Pa})/2$ (Recorded with a Scan Rate of 50 mV/s)

	redox system $R_{red}/R_{ox\,(mV)}$	redox system $S_{red}/S_{ox\,(mV)}$
$Cd_2[Mo(CN)_8]$	590.5	not reversible
$Co_2[Mo(CN)_8]$	600.0	838
$Cr_2[Mo(CN)_8]$	571.5	917
$Cu_2[Mo(CN)_8]$	578.5	880
$Fe_2[Mo(CN)_8]$	560.0	not reversible
$Mn_2[Mo(CN)_8]$	588.0	981
$Ni_2[Mo(CN)_8]$	612.0	873
$Pb_2[Mo(CN)_8]$	581.5	not reversible
$Zn_2[Mo(CN)_8]$	594.0	not reversible

layer (~1 μm), the dR/dE curve tracks the voltammetric curve only in case of peak B_{ox} (Figure 14a). There is no significant change in the reflectance at peak A_{ox}. This indicates that the peak A_{ox} is caused by the oxidation of such small, and therefore probably amorphous, particles, that the light penetrates them without being detectably absorbed, even by the oxidized form. The changes of the optical properties of these particles can only be observed in the case of a thicker substance layer (about 10 μm) (cf. Figure 14b). In that case, the small particles contribute to the diffuse reflection as well. In contrast to the amorphous particles, the conversion of crystalline particles always leads to changed reflectance spectra.

The Electrochemistry of Ag*hcf* in Silver Nitrate Electrolyte. The cyclic voltammograms of silver hexacyanoferrate(II/III) in the presence of silver nitrate solution are very similar for the compounds $Ag_3[Fe(CN)_6]$ and $Ag_4[Fe(CN)_6]$. Figure 10 shows that the cyclic voltammogram, very similar to the octacyanomolybdate, consists of a split and steep peak system B'_{ox}/B'_{red}, the underneath of which is obviously a very broad peak that can be compared to the A_{ox}/A_{red} system of the octacyanomolybdate. A comparison of the cyclic voltammograms recorded in the presence of silver nitrate solution (Figure 10) with the voltammogram recorded in the presence of potassium nitrate solution (Figure 5a) shows that the peak splitting only occurs with the transfer of silver ions. As the powder diffraction patterns (Figure 2, parts a and b) indicate, the reduction of $Ag_3[Fe(CN)_6]$ in the presence of potassium ions does not require any significant change of the lattice. However, the insertion of Ag^+ tremendously changes the lattice structure and crystallinity (cf. Figure 2c). It seems reasonable to assume that a nucleation growth mechanism, similar to the one found for octacyanomolybdate, is responsible.

The Electrochemistry of Solid Octacyanomolybdates of Bivalent Cations. In the presence of potassium nitrate solution, the octacyanomolybdates of the bivalent cations show an electrochemistry (Figure 15) very similar to that of the silver octacyanometalates, which is based upon the following reactions:

Redox system R_{red}/R_{ox}

$$\{M^{II}_{1.5}K[Mo^{IV}(CN)_8]\} \rightleftarrows \{M^{II}_{1.5}[Mo^{V}(CN)_8]\} + K^+ + e^- \quad (16)$$

Redox system S_{red}/S_{ox}

$$2\{M^{II}_2[Mo^{IV}(CN)_8]\} \rightleftarrows 2\{M^{II}_{1.5}[Mo^{V}(CN)_8]\} + M^{2+} + 2e^- \quad (17)$$

The rapidly decreasing response, which is visible in Figure 15 for the case of $Co_2[Mo^{IV}(CN)_8]$, can be explained by the high solubility of the $M^{II}_{1.5}[Mo^{V}(CN)_8]$ compounds and the disintegration of $M^{II}_{1.5}K[Mo^{IV}(CN)_8]$ under a partial dissolution analogous to eq 11.

The formal potential of the peak system R_{red}/R_{ox}, that is, $E_f = (E_{pa}+E_{pc})/2$, of all studied compounds (see Table 2) was close to the formal potential of the dissolved octacyanomolybdate in a 0.1 M KNO_3 solution.

Conclusions

This study of the electrochemical behavior of various solid metal hexacyanoferrates, octacyanomolybdates, and octacyanotungstates revealed that their behavior is governed by some general rules and reaction schemes, which have not been described thus far:

The electrochemical behavior of the studied solid metal cyanometalates in the presence of potassium nitrate solution can be explained on the basis of precipitation equilibria of the involved compounds, as exemplified in the reaction scheme (5).

There is no mixed crystal formation between the two forms of the reduced metal cyanometalates $Me'_3K[X]$ and $Me'_4[X]$ ($Me' = Ag^+$), and $Me''_{1.5}K[X]$ and $Me''_2[X]$ ($Me'' = Me^{2+}$, e.g., Cu^{2+}, Co^{2+}, Cu^{2+}), respectively. Each of these compounds gives its own voltammetric signal, allowing the determination of their ratio in mixtures.

It could be shown that amorphous and crystalline particles of silver octacyanomolybdate and octacyanotungstate samples produce separate oxidation and reduction signals. Although the conversion of the amorphous compounds is thermodynamically controlled, the electrolysis of crystalline constituents is under kinetic control and associated with a nucleation overpotential.

Acknowledgment. Uwe Schröder was supported with a scholarship by Hans-Böckler-Stiftung. The Fonds der Chemischen Industrie is acknowledged for their constant support of the research.

IC9909330